AN ABSTRACT OF THE THESIS OF

Kyle A. Krawl for the degree of Honors Baccalaureate of Science in Geology presented on May 16, 2013. Title: A Geochemical Model for the Petrogenesis of the Curaçao Lava Formation: Implications for the Origin of the Caribbean Plateau.

Abstract approved: _____
Robert A. Duncan

The Curaçao Lava Formation (CLF) records the magmatic and tectonic processes that formed the Caribbean Large Igneous Province (CLIP). A model of the petrogenesis of the CLF was developed using new geochemical and geochronological data. These data include major element compositions obtained using X-ray fluorescence spectroscopy (XRF), trace element concentrations obtained using inductively coupled plasma mass spectrometry (ICP-MS), and radiometric ages obtained using ^{40}Ar-^{39}Ar dating. The wide range of ^{40}Ar-^{39}Ar ages (62.3 ± 0.8 Ma to 92.0 ± 1 Ma) obtained for the Curaçao lavas contradicts previous models suggesting that the CLF formed in 1-2 million years. Crystallization modeling indicates that the lavas, sills and hyaloclastites of the CLF could have formed by fractional crystallization of parental magmas with similar major element compositions. The persistently flat rare earth element patterns of the Curaçao lavas can be reproduced by 10-30% partial melting of a predominately depleted mantle source with a minor (1.4-3.4%) enriched component. These results are consistent with a petrogenetic model for the CLIP in which lateral displacement of mantle plume head material beneath the Caribbean plateau as a result of subduction-driven mantle flow allows for the generation of magmas from an essentially homogenous mantle source over approximately 30 million years.

Key Words: Caribbean plateau, large igneous province, mantle plume, geochemistry

Corresponding email address: kyle.krawl@gmail.com

A Geochemical Model for the Petrogenesis of the Curaçao Lava Formation: Implications for the Origin of the Caribbean Plateau

by

Kyle A. Krawl

A PROJECT

submitted to

Oregon State University

University Honors College

in partial fulfillment of
the requirements for the
degree of

Honors Baccalaureate of Science in Geology (Honors Scholar)

Presented May 16, 2013
Commencement June 2013

Honors Baccalaureate of Science in Geology project of Kyle A. Krawl presented on May 16, 2013.

APPROVED:

_____

Mentor, representing College of Earth, Ocean and Atmospheric Sciences

_____

Committee Member, representing College of Earth, Ocean and Atmospheric Sciences

_____

Committee Member, representing College of Earth, Ocean and Atmospheric Sciences

_____

Program Head, Geology

_____

Dean, University Honors College

I understand that my project will become part of the permanent collection of Oregon State University, University Honors College. My signature below authorizes release of my project to any reader upon request.

_____

Kyle A. Krawl, Author

ACKNOWLEDGEMENTS

This research would not have been possible without the aid of several individuals. Bob Duncan and Adam Kent provided me with the resources and guidance necessary to complete this thesis. Matt Loewen provided extensive help with sample preparation, data collection and modeling. Frank Tepley and Dale Burns assisted with EMPA, and John Huard assisted with ^{40}Ar-^{39}Ar analyses. XRF analyses were provided by Chris Sinton (University of Redlands) and Jade Star Lackey (Pomona College). ICP-MS and additional XRF analyses were provided by the Washington State University Geoanalytical Lab. This research was funded by National Science Foundation grant OCE 1028707 (to Duncan and Kent).

TABLE OF CONTENTS

LIST OF FIGURES AND TABLES

LIST OF FIGURES AND TABLES (Continued)

A Geochemical Model for the Petrogenesis of the Curaçao Lava Formation: Implications for the Origin of the Caribbean Plateau

BACKGROUND

The Caribbean Plateau

The Caribbean plateau is a large igneous province (LIP)—a massive emplacement of intrusive and extrusive igneous rock (Coffin and Edholm, 1994). A popular model attributes the petrogenesis of LIPs to melting triggered by upwelling associated with mantle plumes during the initial stages of hotspot activity (Morgan, 1981; Richards et al., 1989; Duncan and Richards, 1991). According to this model, LIPs form over a geologically short period of time—typically within a few million years (Morgan, 1981; Richards et al., 1989; Duncan and Richards, 1991).

The majority of plate tectonic models suggest that the Caribbean Large Igneous Province (CLIP) moved into its present position from the east Pacific region and that this eastward movement began during the late Cretaceous (Burke et al., 1984; Duncan and Hargraves, 1984; Pindell and Barrett, 1990; Kerr et al., 1999). Duncan and Hargraves (1984) report that this eastward movement resulted in the collision of the CLIP with the Greater Antilles Arc between South and Central America between 80 and 90 Ma. According to these authors, this resulted in the uplift and accretion of thick sections of the Caribbean plateau crust along the margins of northwestern South America. Rather than being subducted, the CLIP was sufficiently thick and buoyant to clog the trench. This resulted in a polarity flip of the Greater Antilles Arc (from northeast-dipping to southwest-dipping), accompanied by subduction of oceanic crust beneath the eastern

margin of the Caribbean plateau. By about 60 Ma, the Central America Arc had formed to the southwest of the CLIP, resulting in the subduction of the Farallon plate beneath the Caribbean Plateau (Duncan and Hargraves, 1984).

The Curaçao Lava Formation

The island of Curaçao (**Figure 1**) contains some of the best-preserved subaerial sections of the Caribbean plateau, and the petrology and stratigraphy of this region are well-documented. Klaver (1987) determined that the Curaçao Lava Formation (CLF) is more than 5 km thick, and composed predominately of massive and pillow lavas, hyaloclastites and sills. The lower half of the exposed section is dominated by olivine basalts and picrites, some containing as much as 31 wt% MgO (Beets et al., 1982). Kerr et al. (1996) suggest that the high-MgO picrites are olivine cumulates. The upper half of the CLF consists of more evolved plagioclase- and clinopyroxene-phyric pillow basalts, dolerite sills, and hyaloclastites (Klaver, 1987). Kerr et al. (1996) concluded that the picrites of the CLF are related to the basalts by simple fractional crystallization of olivine, clinopyroxene, and plagioclase. Révillon et al. (1999), however, found that trends on trace element variation diagrams indicated that fractional crystallization alone cannot explain the relationship between the basalts and picrites.

Stratigraphic relationships and radiometric ages from previous research suggest that the lavas of the CLF were formed relatively rapidly. Only one intercalation of pelagic sediments has been found within the CLF, suggesting that the extrusion of the lavas occurred during a short timeframe (Klaver, 1987). Previous ^{40}Ar-^{39}Ar ages for lavas range from 88 to 90 Ma (Sinton et al., 1998). A Re-Os isochron age of 85 ± 8.1 Ma has

also been obtained for a Curaçao lava flow (Walker et al., 1999). Previous geochronological analyses suggest that the Caribbean plateau formed as a result of two large-scale magmatic pulses (Sinton et al., 1998). Kerr et al. (1996) report that most of the Curaçao lavas possess nearly constant Nd isotopic ratios (ε_{Nd}~ +6-7) and flat rare-earth element (REE) patterns. However, REE and isotopic data collected by Sinton et al. (1998) suggest that the formation of the oceanic plateau involved two compositionally distinct mantle sources and variable melting conditions.

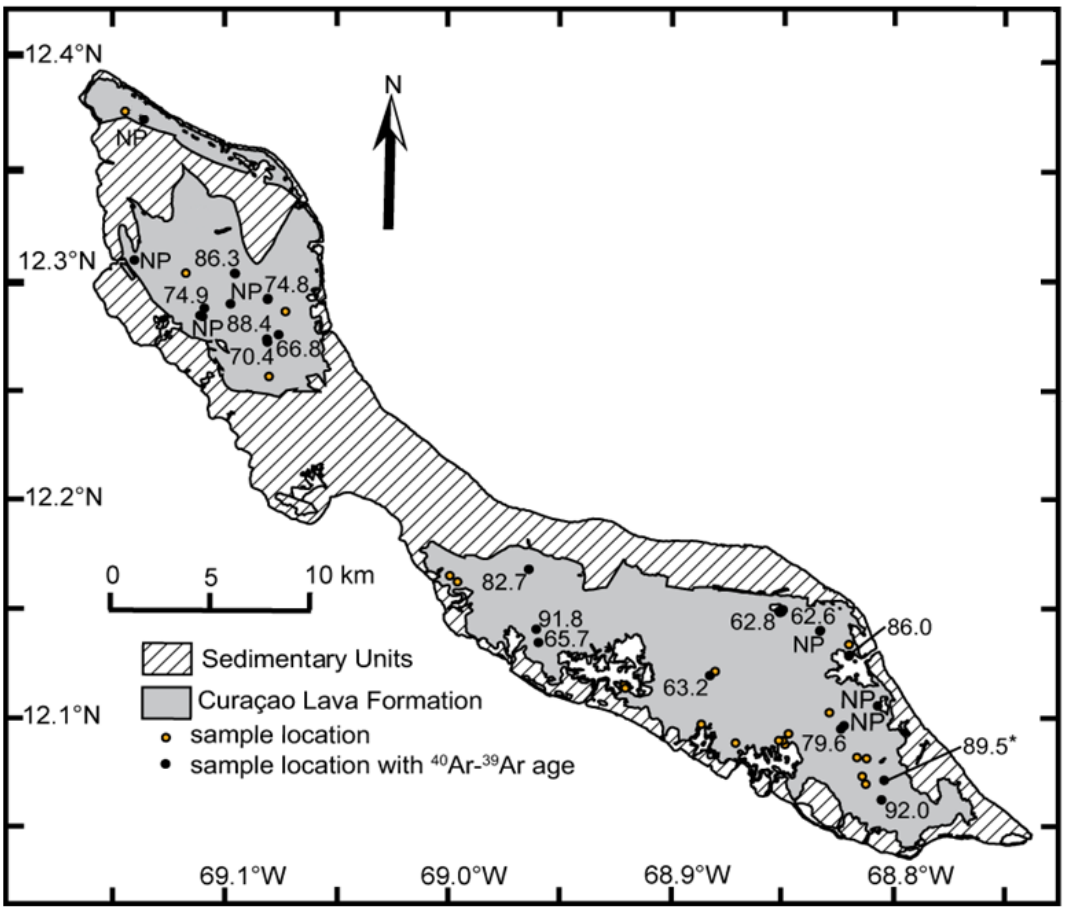

Figure 1. Map of Curaçao (adapted from Loewen et al., in review). Sample locations and ages (in Ma) are shown, including one previous ^{40}Ar-^{39}Ar age from Sinton et al. (1998) shown with an asterisk.

The majority of models for the petrogenesis of the CLF suggest the involvement of a mantle plume, but have until recently relied on a relatively limited set of geochemical and geochronological data. The ^{40}Ar-^{39}Ar dating attempts by Sinton et al. (1998) produced only three successful plateau ages. Additionally, varying interpretations of geochemical data obtained from the rocks of Curaçao have resulted in models using a number of different mantle source compositions and parental magma compositions (e.g. Klaver 1987; Sinton et al., 1998; Kerr et al.; 1996). The model presented here incorporates a significant number of new reliable plateau ages and major and trace element chemical data for Curaçao lavas (Loewen et al., in review). Previous models indicating that the CLIP formed at 88-90 Ma from melting associated with the arrival of a mantle plume beneath the lithosphere cannot adequately explain the observed geochronological and geochemical variation of the rocks of the CLF. The new model proposed herein provides parental magma and mantle source compositions that are consistent with the full range of ages and compositions observed for CLF rocks.

METHODS

Fifty-six samples collected from the CLF by R. A. Duncan and M. Loewen form the basis of this research. Samples were examined in thin section and divided into groups based on differences in mineral assemblage and texture. Samples in which mineral phases were unidentifiable due to alteration were excluded from further analysis.

Major and trace element data were collected for selected samples using X-ray fluorescence spectroscopy (XRF) by Dr. Chris Sinton at the University of Redlands. Additional major element data were collected using XRF by the Washington State University Geoanalytical Lab. Rare earth and trace element data were collected using inductively coupled plasma mass spectrometry (ICP-MS) at the Washington State University Geoanalytical Lab.

Major and trace element data were collected for olivine, plagioclase, and clinopyroxene using Electron Microprobe Analysis (EMPA). EMPA was conducted at Oregon State University using a Cameca SX-100 Electron Microprobe equipped with 5 wavelength dispersive spectrometers (WDS), one energy dispersive spectrometer (EDS), and a high speed back scattered electron (BSE) imaging system. A total of 44 olivine crystals, 69 pyroxene crystals and 58 plagioclase crystals were analyzed in eight of the Curaçao samples (two picrites, two poikilitic sills and four plagioclase-clinopyroxene tholeiites) at a spot size of 1 μm, a beam intensity of 30 nA and an acceleration voltage of 15 kV.

Age determinations of groundmass and plagioclase separates were performed at Oregon State University using standard ^{40}Ar-^{39}Ar incremental heating techniques.

Samples were crushed, sieved, washed and subjected to mild acid leaching with HCl and HNO_3 prior to irradiation. Neutron flux during irradiation was monitored using FCT-3 biotite (28.02 Ma; Renne et al., 1998). Argon isotopic compositions of samples were determined using a Mass Analyzer Products (MAP) 215-50 mass spectrometer attached to a low-blank, all-metal extraction line. Samples were heated using a continuous 10W CO_2 laser operated as a defocused beam. Incremental heating plateau ages and isochron ages were calculated for each sample using the ArArCALC v2.2 software package (after Koppers, 2002).

Parental magma evolution was modeled using the MELTS software package (Ghiorso and Sack, 1995). MELTS models the evolution of magmas in a series of steps of varying temperature and/or pressure based on thermodynamic properties, and characterizes equilibrium and fractional crystallization by producing a liquid line of descent. Crystallization was modeled at a constant pressure of 1 kbar using the mineral redox buffer quartz-fayalite-magnetite (QFM) to constrain oxygen fugacity. The starting composition used for the model is shown in **Table 1**. This initial composition was estimated using the range of major element concentrations observed for CLF picrites.

In order to determine the mantle source composition and melting conditions that formed the primary magma of the CLF, a batch melting model was developed. The model calculates concentrations of selected rare earth elements (REEs) present in a liquid derived from a given percent of partial melt of a specified mantle source. Mantle source compositions and crystal-liquid partition coefficients used in the model were adapted from Gurenko and Chaussidon (1995).

Table 1. Starting composition used in MELTS models expressed as wt% of oxides. In models with different water contents, concentrations were renormalized to total 100%. Total iron content is expressed as Fe_2O_3 (relative amounts of Fe^{2+} and Fe^{3+} are modeled using different redox buffers).

Oxide	wt %
SiO_2	47.251
TiO_2	0.537
Al_2O_3	8.376
Fe_2O_3	11.297
MgO	23.625
MnO	0.161
Cr_2O_3	0.322
CaO	7.195
K_2O	0.054
Na_2O	0.966
P_2O_5	0.107
H_2O	0.107

RESULTS

Petrography

Of the 33 thin sections examined using petrographic analysis, 28 had clearly identifiable mineralogies. Among these 28 samples three unique rock types were identified—picrites, poikilitic sills, and plagioclase-clinopyroxene tholeiites. Five samples were classified as picrites, five as poikilitic sills, and 18 as plagioclase-clinopyroxene tholeiites. Four of the plagioclase-clinopyroxene tholeiites with significant amounts of altered glass were further classified as hyaloclastites. Images of thin sections from each category are shown in **Figure 2**.

The picrites are composed of 40-70 vol. % olivine, 5-15 vol. % clinopyroxene, and 5-10 vol. % spinel. Olivine phenocrysts have sizes of 0.125-5 mm, and are predominately euhedral to subhedral. Hexagonal and rounded morphologies are common, and rare spinifex crystals were also observed. Nearly all of the olivine crystals have been at least partially altered to iddingsite. Clinopyroxene phenocrysts have sizes of up to 2.5 mm, and are predominately euhedral to subhedral. Crystal morphology varies greatly, and includes feathery quench growths as well as skeletal and tabular phenocrysts. Spinel phenocrysts have sizes of up to 0.25 mm. Crystals are predominately euhedral, and exhibit either blocky or elongate morphologies. Spinel phenocrysts were observed both within and between olivine grains, and in the latter case were often grouped together in branching chains.

The poikilitic sills are composed of 25-60 vol. % clinopyroxene, 20-60 vol. % plagioclase, and 5-10 vol. % spinel. Clinopyroxene phenocrysts have sizes of 0.125-2

mm. Crystals are predominately subhedral, and exhibit blocky, tabular and occasionally partially rounded morphologies. Subophitic and ophitic clinopyroxene is common, often forming almost radial clusters with plagioclase crystals. Plagioclase phenocrysts have sizes of 0.05-4.5 mm. Both ophitic and subophitic plagioclase is present. Crystals are predominately subhedral, and exhibit blocky, tabular, and needle morphologies. Plagioclase crystals in several samples have been at least partially altered to sericite. Spinel phenocrysts have sizes of 0.05-1.25 mm. Crystals are predominately euhedral, and exhibit both compact and elongate morphologies. Spinel phenocrysts were observed both within and between clinopyroxene and plagioclase grains. Chlorite was commonly present as an alteration product, and composed up to 5 vol. % of the more pervasively altered samples.

The plagioclase-clinopyroxene tholeiites are composed of 1-50 vol. % clinopyroxene, 5-70 vol. % plagioclase, and 5-10 vol. % spinel. Clinopyroxene phenocrysts have sizes of 0.02-1.25 mm. Crystals are predominately subhedral to anhedral, exhibiting blocky, tabular, and occasionally rounded morphologies. Plagioclase phenocrysts have sizes of 0.1-3 mm. Crystals are predominately subhedral to anhedral, and exhibit both tabular and needle-like morphologies. Spinel phenocrysts have sizes of 0.02-0.400 mm. As in the sills, crystals are predominately euhedral, and exhibit both compact and elongate morphologies. The predominant alteration products are chlorite (up to 5 vol. %) and sericite (up to 1 vol. %).

The hyaloclastites are composed of 5-10 vol. % plagioclase and clinopyroxene and up to 90 vol. % glass, with less than 1 vol. % spinel. Nearly all of the glass in the hyaloclastites has been altered to palagonite. Plagioclase crystals are euhedral, present as

tabular and needle-like phenocrysts with sizes of 0.125-1.25 mm and as glomerocrysts of up to 3 mm. Clinopyroxene is rare, and occurs as subhedral to euhedral crystals with sizes of up to 0.75 mm.

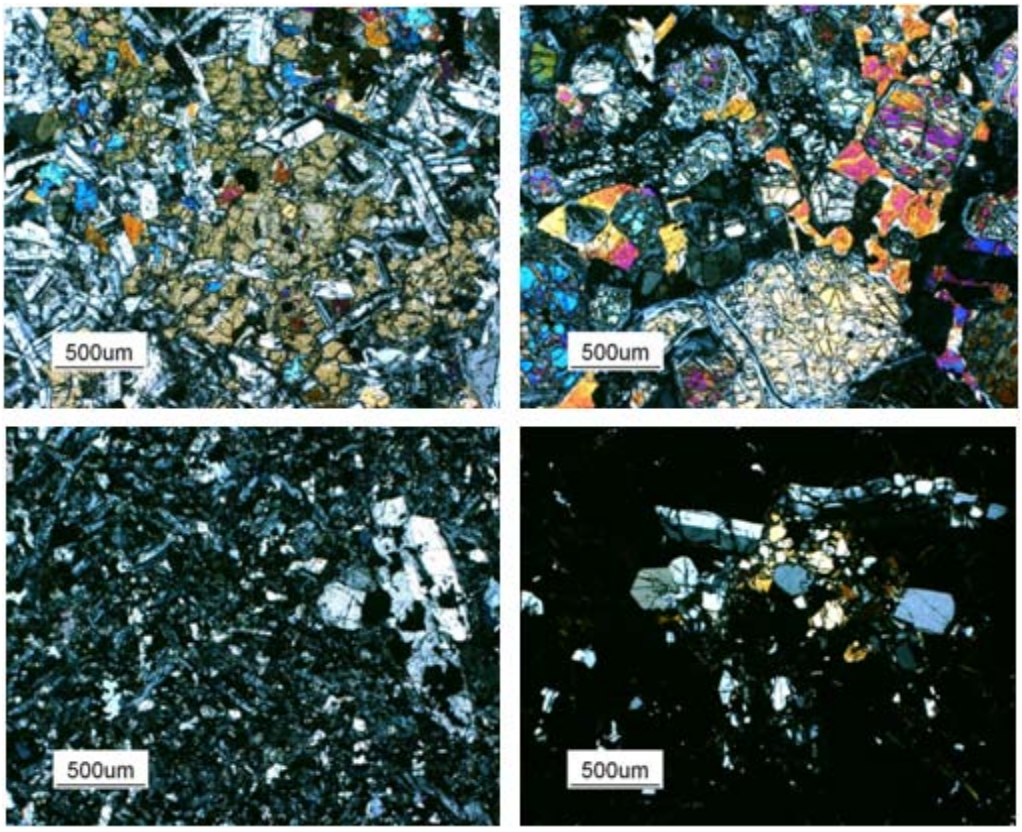

Figure 2. Images from CLF sample thin sections. Sample CAO 13 (upper left) is a sill, sample CAO 15a (upper right) is a picrite, sample CAO 22 (lower left) is a tholeiite, and sample CAO 35d (lower right) is a hyaloclastite.

Geochronology

^{40}Ar-^{39}Ar ages obtained for 22 samples, including 15 tholeiites, four sills and three hyaloclastites, are summarized in **Table 2**. Reliable plateau ages range from 62.3 to 92.0 Ma for tholeiites, from 83.9 to 91.8 Ma for sills, and from 86.3 to 88.4 Ma for

hyaloclastites. Full age spectra are available from Loewen et al. (in review). These ages cover a significantly larger range than the ages of 88-90 Ma previously reported by Sinton et al. (1998).

Table 2. ^{40}Ar-^{39}Ar data for CLF samples. Ages were calculated using biotite monitor FCT-3 (28.02 Ma; Renne et al., 1998) and the total decay constant $\lambda = 5.530 \times 10^{-10}$ yr^{-1} (Steiger and Jäger, 1977). N is the number of heating steps (steps in plateau/total). MSWD is a statistical comparison of variance within step ages with variance with respect to the plateau age. Material abbreviations are grdnms = groundmass, plag = plagioclase, and wr = whole rock.

Sample	Material	Total Fusion Age (Ma)	2s error	Plateau Age (Ma)	2s error	N	% ^{39}Ar	MSWD	Isochron Age (Ma)	2s error	Initial $^{40}Ar/^{36}Ar$	2s error
Cur 21i	grndms	92.0	1.5	92.0	1.0	6/10	86	2.32	91.9	1.0	295.9	2.4
Cao 40b	plag	91.5	1.7	91.8	2.1	7/7	100	1.72	90.5	3.2	299.2	8.7
Cao 07	glass	87.4	2.3	88.4	2.1	9/10	98	0.61	83.2	22.9	318.5	106.0
Cao 35d	glass	86.0	2.8	86.3	2.4	10/10	100	0.54	89.0	6.1	278.6	32.5
Cao 13	plag	85.7	3.0	86.0	1.9	7/7	100	0.44	86.0	1.9	295.1	1.6
Cao 18	plag	83.9	1.7	83.9	1.6	7/7	100	0.40	83.4	2.1	296.5	3.6
79 Be-069	grndms	74.4	4.6	79.6	3.6	8/10	83	0.35	77.6	6.1	296.5	2.7
BK 79-262	grndms	73.7	2.6	74.9	2.1	10/10	100	0.78	77.8	4.1	288.6	8.1
Cao 20	grndms	74.1	2.3	74.2	2.4	9/10	96	1.56	72.9	2.5	298.8	3.8
Cao 04a	grndms	69.1	1.2	70.2	1.1	10/11	94	0.82	70.7	2.5	294.0	5.7
Cao 03	grndms	66.3	0.9	66.7	0.8	12/12	100	1.20	67.2	1.2	294.3	2.2
BK 79-118	grndms	65.5	2.9	65.7	2.4	10/10	100	0.85	68.0	3.8	293.8	2.2
Cao 30	grndms	63.2	1.0	62.8	1.0	9/12	88	1.42	62.5	2.1	296.2	7.0
Cur 10-02	grndms	62.6	0.8	63.0	1.0	10/12	89	1.91	63.8	2.4	291.1	10.7
Cao 10	grndms	60.1	0.8	62.3	0.8	8/12	84	1.74	64.6	1.7	281.5	9.0
Cao 14	plag	97.5	3.0	79.4	1.9	6/7	68	1.62	81.0	8.6	291.7	19.7
BK 79-183	grndms	53.4	10.8	66.4	10.7	5/9	68	0.38	71.0	22.5	292.3	13.0
BK 79-163	grndms	41.2	2.9	41.6	2.6	5/11	37	0.24	50.9	107.0	293.3	25.2
Cao 32	grndms	118.0	3.5	83.8	4.4	6/10	28	1.54	88.7	5.3	262.5	26.2
Cao 22	grndms	72.4	0.5	70.1	0.5	6/14	31	0.62	70.1	1.3	294.6	22.6
Cao 21	grndms	61.2	0.7	N/A	-	-	-	-	N/A	-	-	-
BK 79-263	glass	53.1	1.5	N/A	-	-	-	-	N/A	-	-	-

Geochemistry

Concentrations of major and trace elements collected for 29 samples are shown in **Table 3** and **Table 4** (respectively). Samples identified as picrites are composed of 21.4 to 29.1 wt% MgO and 41.1 to 44.1 wt% SiO_2. Poikilitic sills are composed of 7.4 to 9.0 wt% MgO and 44.1 to 51.4 wt% SiO_2. Tholeiites are composed of 7.7 to 9.3 wt% MgO and 49.9 to 51.4 wt% SiO_2. In general, the compositions of the picrites, sills, and

tholeiites fall within the range of compositions reported by Klaver (1987) for samples with similar petrographic characteristics.

Table 3. Major element concentrations for selected CLF samples in wt%. Data were obtained using XRF. Concentrations are expressed as weight percent of oxides. Total iron concentrations are expressed as wt% of iron (III) oxide ($Fe_2O_3^*$). Samples without a listed type were not examined in thin section.

Sample	Type	SiO_2	TiO_2	Al_2O_3	$Fe_2O_3^*$	MnO	MgO	CaO	Na_2O	K_2O	Total
CAO 15	Picrite	41.10	0.39	5.62	11.32	0.17	29.09	5.49	0.05	0.02	93.39
CAO 16	Picrite	44.02	0.56	8.64	10.64	0.17	22.26	7.62	1.11	0.06	96.33
CAO 17	Picrite	44.07	0.58	8.77	10.52	0.16	21.44	7.60	0.86	0.06	95.07
CAO 24	Picrite	44.11	0.45	7.42	11.25	0.17	27.00	6.63	0.50	0.02	98.13
CAO 10	Sill	50.75	1.06	14.84	11.56	0.18	8.57	11.92	2.49	0.32	100.60
CAO 13	Sill	49.12	0.65	15.57	8.99	0.16	9.00	13.82	1.73	0.06	100.98
CAO 14	Sill	49.08	0.95	13.98	10.99	0.18	8.20	11.38	2.61	0.11	100.30
CAO 18	Sill	50.44	1.14	14.21	11.83	0.20	7.53	11.19	1.96	0.06	100.70
CAO 40B	Sill	51.41	1.20	13.73	12.87	0.20	7.63	11.70	1.81	0.11	102.70
CUR 10-5a	Sill	50.58	1.22	13.90	12.59	0.20	7.38	9.99	3.66	0.05	103.39
CAO 19	Tholeiite	49.93	1.02	14.45	11.17	0.17	7.68	10.67	3.17	0.37	102.28
CAO 20	Tholeiite	51.18	1.21	13.78	11.64	0.18	6.85	11.35	2.50	0.07	101.45
CAO 21	Tholeiite	49.69	0.87	14.40	10.38	0.17	8.45	11.15	3.02	0.27	101.80
CAO 22	Tholeiite	47.44	0.92	13.88	11.02	0.19	8.76	10.18	2.73	0.94	99.94
CAO 26	Tholeiite	50.01	0.86	13.09	9.85	0.17	8.66	13.79	1.54	0.07	99.74
CAO 27	Tholeiite	50.62	0.87	13.48	10.13	0.17	9.35	12.09	2.46	0.14	102.00
CAO 3	Tholeiite	49.94	1.21	13.83	12.01	0.19	6.98	9.90	3.47	0.28	101.71
CAO 30	Tholeiite	49.96	1.02	14.05	11.07	0.18	8.38	11.98	2.58	0.24	102.38
CAO 32	Tholeiite	49.98	1.20	13.37	12.58	0.19	7.11	10.77	1.83	0.09	99.15
CAO 40A	Tholeiite	51.27	1.04	14.05	11.39	0.19	8.01	12.45	1.80	0.04	102.18
CAO 4A	Tholeiite	49.13	0.97	13.52	10.90	0.17	8.26	11.37	3.01	0.18	100.82
CUR 10-07	Tholeiite	50.64	0.91	13.60	10.44	0.16	8.29	11.74	2.76	0.11	101.60
CUR 10-09	Tholeiite	51.41	0.89	14.01	10.33	0.18	8.59	12.05	2.51	0.08	102.74
CUR 10-3b	Tholeiite	50.27	0.86	13.55	10.20	0.18	9.05	12.71	2.45	0.03	101.88
CUR-10-02	Tholeiite	50.88	1.01	14.01	10.88	0.17	7.94	10.78	3.32	0.19	102.83
CAO 23	-	50.24	0.73	12.68	9.88	0.19	9.18	13.93	1.86	0.03	100.70
CAO 31	-	47.10	0.76	12.27	8.83	0.16	7.92	18.55	0.12	0.03	95.97
CAO 39	-	44.42	0.78	14.70	8.94	0.15	6.56	19.92	0.19	0.02	95.98
CAO 41	-	48.91	0.92	14.03	10.89	0.19	9.68	11.75	1.80	0.07	100.20
CUR 10-11	-	43.67	0.54	8.31	10.58	0.16	22.83	7.37	0.98	0.05	95.60

Table 4. Trace element concentrations for selected CLF samples. Data were obtained using ICP-MS. Concentrations are in ppm.

Sample	La	Ce	Pr	Nd	Sm	Eu	Gd	Tb	Dy	Ho	Er	Tm	Yb	Lu	Ba	Th	Ta	U	Pb	Rb	Cs	Sr	Sc	Zr	Y	Nb	Hf
CAO 10	2.76	7.33	1.16	5.95	2.05	0.81	2.87	0.55	3.60	0.78	2.16	0.32	1.98	0.32	15.04	0.23	0.27	0.08	0.63	0.74	0.00	224.36	49.77	49.74	19.14	3.55	1.43
CAO 13	1.65	4.39	0.71	3.73	1.37	0.56	1.84	0.36	2.36	0.52	1.42	0.21	1.32	0.21	7.85	0.13	0.15	0.05	0.48	0.44	0.00	88.17	45.28	30.29	12.78	2.13	0.89
CAO 14	2.33	6.11	0.97	4.98	1.77	0.75	2.53	0.48	3.26	0.71	1.97	0.29	1.81	0.29	9.86	0.20	0.21	0.07	0.60	1.28	0.01	90.77	48.46	41.96	17.15	2.85	1.23
CAO 15	1.18	2.99	0.46	2.30	0.78	0.31	1.04	0.19	1.29	0.28	0.76	0.11	0.68	0.11	3.70	0.10	0.09	0.03	0.08	0.62	0.02	12.90	22.54	18.18	6.72	1.34	0.53
CAO 16	1.85	4.77	0.72	3.57	1.19	0.48	1.63	0.29	1.95	0.42	1.17	0.17	1.04	0.17	11.81	0.17	0.15	0.05	0.24	2.37	0.01	60.09	29.87	28.06	10.31	2.16	0.80
CAO 17	1.98	5.05	0.77	3.79	1.26	0.50	1.66	0.30	2.06	0.44	1.19	0.17	1.09	0.17	25.54	0.19	0.16	0.05	0.20	3.39	0.15	95.36	30.24	29.04	10.60	2.24	0.85
CAO 18	3.28	8.19	1.23	6.25	2.14	0.89	2.96	0.56	3.88	0.84	2.34	0.35	2.18	0.35	7.19	0.27	0.28	0.11	1.06	0.55	0.00	80.80	48.51	52.36	20.68	3.97	1.54
CAO 19	2.74	7.27	1.16	5.99	2.08	0.85	3.01	0.58	3.93	0.83	2.36	0.34	2.17	0.34	27.82	0.23	0.22	0.09	0.86	7.82	0.11	288.09	47.35	51.22	20.70	3.09	1.51
CAO 20	3.32	8.54	1.30	6.77	2.34	0.90	3.23	0.61	4.09	0.90	2.54	0.37	2.35	0.38	24.91	0.28	0.31	0.10	0.82	0.96	0.01	123.49	48.21	56.39	22.34	4.29	1.63
CAO 21	2.35	6.24	1.00	5.08	1.76	0.71	2.49	0.49	3.28	0.72	2.03	0.31	1.91	0.31	11.65	0.21	0.19	0.06	0.20	2.71	0.24	151.43	47.84	40.90	16.73	2.63	1.21
CAO 22	3.49	9.36	1.55	8.03	2.63	0.94	3.19	0.55	3.44	0.72	1.99	0.28	1.75	0.27	242.90	0.48	0.16	0.24	0.66	12.55	0.07	267.02	45.84	43.51	18.00	2.38	1.32
CAO 22B	7.87	16.67	2.29	9.85	2.34	0.87	2.29	0.36	2.17	0.43	1.21	0.17	1.10	0.18	355.67	1.01	0.19	0.37	1.26	15.83	0.09	448.66	16.49	63.96	11.16	2.67	1.76
CAO 23	2.48	6.24	0.95	4.62	1.53	0.61	2.13	0.40	2.75	0.60	1.67	0.25	1.54	0.25	10.34	0.27	0.22	0.19	2.83	0.53	0.00	56.95	42.45	36.58	14.78	3.08	1.05
CAO 24	1.48	3.79	0.59	2.87	0.98	0.37	1.29	0.24	1.62	0.34	0.97	0.14	0.87	0.14	5.33	0.15	0.12	0.04	0.19	1.00	0.01	38.87	25.66	22.69	8.49	1.71	0.64
CAO 26	3.01	7.46	1.13	5.65	1.81	0.70	2.43	0.46	3.05	0.65	1.77	0.26	1.64	0.26	15.23	0.28	0.24	0.08	0.26	0.90	0.01	91.55	43.28	43.21	16.10	3.51	1.23
CAO 27	3.25	7.90	1.17	5.70	1.91	0.71	2.44	0.46	3.12	0.65	1.81	0.26	1.65	0.27	25.05	0.29	0.25	0.09	0.24	1.64	0.01	95.77	44.27	43.44	16.32	3.71	1.25
CAO 3	3.25	8.40	1.32	6.79	2.34	0.90	3.22	0.62	4.15	0.89	2.53	0.37	2.30	0.38	17.56	0.29	0.29	0.09	0.19	3.56	0.02	119.94	48.14	56.52	22.73	4.15	1.62
CAO 30	2.65	7.09	1.12	5.76	2.00	0.78	2.79	0.53	3.56	0.76	2.09	0.31	1.92	0.31	11.01	0.23	0.24	0.06	0.20	0.66	0.01	221.89	47.89	47.90	18.59	3.31	1.36
CAO 31	2.93	6.94	1.04	5.07	1.68	0.71	2.22	0.41	2.69	0.58	1.59	0.23	1.43	0.22	5.45	0.25	0.21	0.07	0.45	0.18	0.01	11.69	35.88	38.24	14.06	2.94	1.09
CAO 32	2.98	7.70	1.22	6.28	2.24	0.84	2.98	0.58	3.97	0.86	2.39	0.35	2.24	0.36	20.49	0.28	0.27	0.08	0.33	1.03	0.01	133.29	49.53	52.32	21.05	3.77	1.55
CAO 36	15.48	31.19	4.06	16.40	3.85	1.20	3.94	0.66	4.26	0.86	2.37	0.35	2.16	0.34	1078.92	4.10	0.43	1.21	6.60	28.31	1.37	363.64	20.88	142.35	22.08	6.05	3.86
CAO 39	3.49	7.97	1.13	5.57	1.73	0.76	2.31	0.42	2.87	0.60	1.66	0.25	1.51	0.25	7.01	0.34	0.26	0.13	2.82	0.36	0.03	19.21	40.81	40.89	15.06	3.63	1.17
CAO 40A	3.41	8.67	1.34	6.67	2.20	0.87	3.01	0.56	3.74	0.80	2.20	0.32	2.00	0.32	10.61	0.34	0.30	0.12	1.09	0.37	0.01	92.93	48.66	51.93	19.53	4.07	1.52
CAO 40B	3.78	9.91	1.55	7.70	2.64	0.97	3.44	0.64	4.23	0.91	2.54	0.38	2.35	0.38	23.42	0.38	0.35	0.15	1.12	1.42	0.01	90.57	48.02	62.22	22.67	4.78	1.78
CAO 41	3.04	7.66	1.18	5.85	1.93	0.76	2.63	0.49	3.20	0.69	1.98	0.28	1.77	0.28	12.31	0.26	0.25	0.13	1.91	0.79	0.00	86.24	44.36	47.02	17.23	3.54	1.35
CAO 4A	2.57	6.76	1.10	5.65	2.01	0.77	2.65	0.52	3.41	0.74	2.04	0.30	1.83	0.31	21.02	0.22	0.22	0.07	0.16	1.80	0.01	101.85	46.95	46.40	18.60	3.14	1.31
CUR 10-07	2.32	6.17	1.00	5.20	1.85	0.74	2.57	0.49	3.26	0.70	1.98	0.29	1.80	0.30	8.33	0.19	0.21	0.06	0.17	0.64	0.00	179.67	47.52	43.16	17.46	2.85	1.27
CUR 10-09	3.26	7.96	1.19	5.71	1.84	0.73	2.48	0.47	3.07	0.66	1.85	0.27	1.69	0.26	21.83	0.32	0.25	0.09	0.27	1.04	0.00	152.86	45.12	43.89	16.44	3.77	1.25
CUR 10-11	1.81	4.61	0.71	3.50	1.15	0.47	1.56	0.28	1.87	0.40	1.10	0.17	1.00	0.16	13.88	0.16	0.14	0.05	0.16	2.47	0.06	73.08	29.17	27.13	9.95	2.07	0.77
CUR 10-3b	2.99	7.33	1.11	5.51	1.81	0.70	2.43	0.45	3.01	0.64	1.80	0.26	1.64	0.26	10.21	0.27	0.22	0.07	0.24	0.36	0.00	97.86	43.46	42.44	15.94	3.27	1.19
CUR 10-5a	3.35	8.77	1.36	6.87	2.38	0.92	3.31	0.63	4.23	0.92	2.60	0.38	2.40	0.38	5.70	0.30	0.30	0.08	0.27	0.58	0.01	155.13	50.76	58.10	22.96	4.22	1.71
CUR-10-02	2.77	7.34	1.17	6.01	2.12	0.85	2.92	0.56	3.76	0.80	2.27	0.33	2.08	0.32	26.02	0.31	0.20	0.07	0.20	2.76	0.02	156.87	46.76	49.23	20.14	2.91	1.43

Olivine crystals analyzed using EMPA have forsterite contents of 81-89, with a mean composition of Fo_{87} (**Figure 3**). These values are similar to those reported by Klaver (1987) (Fo 85-90). Olivine crystals with hexagonal and spinifex morphologies show little compositional variation (Fo 87-89) between rim and core. Rounded crystals tend to show slight compositional zoning, exhibiting rims with lower forsterite contents (Fo 81-86) than the cores (Fo 86-89).

Plagioclase crystals have compositions of An 88-60, with a mean composition of An_{73} (**Figure 3**). Plagioclase crystals in the poikolitic sills have, on average, lower anorthite content (mean composition An_{71}) than plagioclase in the tholeiites (mean composition An_{76}).

Clinopyroxene crystals compositions have ranges of En 34-70, Fs 9-40, and Wo 20-46, with a mean composition of $En_{49}Fs_{16}Wo_{45}$ (**Figure 4**). Clinopyroxene crystals in the picrites tend to be closer in composition to diopside (mean composition of $En_{44}Fs_{13}Wo_{43}$) than clinopyroxene found in the tholeiites and sills (mean composition of $En_{49}Fs_{17}Wo_{34}$).

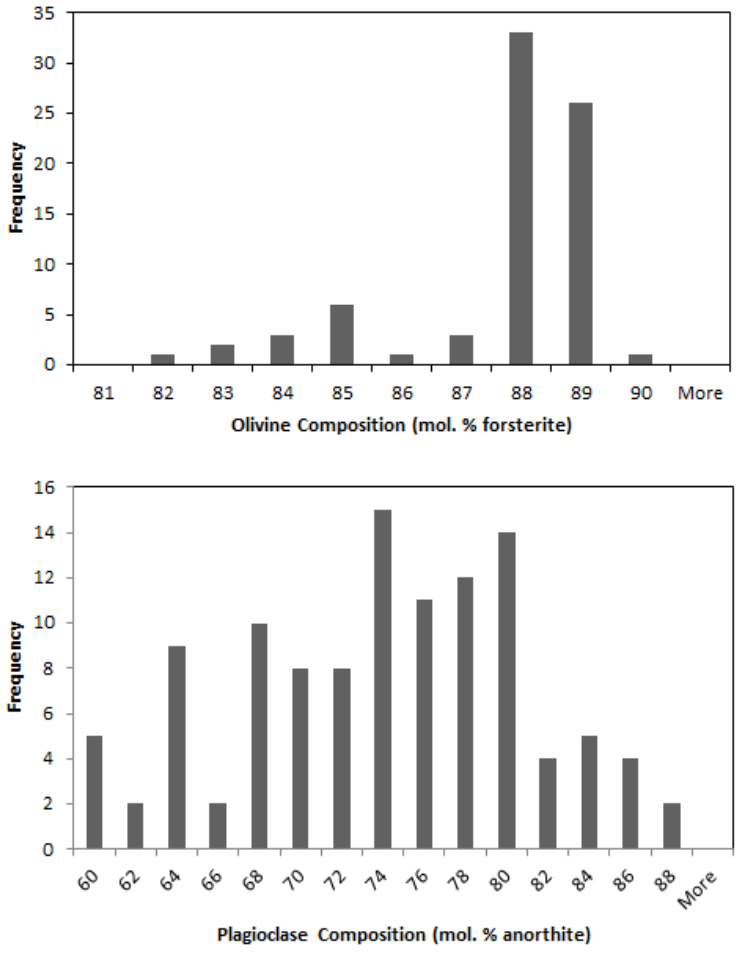

Figure 3. Histograms of olivine (top) and plagioclase (bottom) compositions.

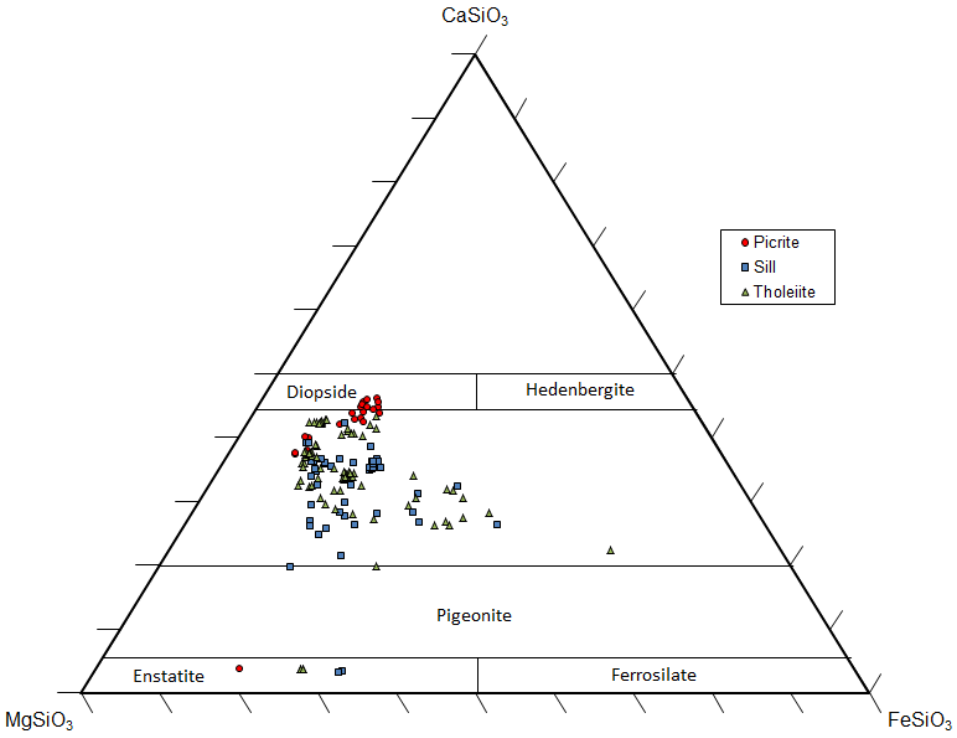

Figure 4. Enstatite-Wollastonite-Ferrosilate ternary diagram of pyroxene crystals in CLF picrites, sills, and tholeiites. Plotted using TriPlot (after Graham and Midgley, 2000).

DISCUSSION

Timing of CLF Magmatism

If the bulk of the CLF was formed during a single melting event associated with the arrival of a mantle plume at 88-90 Ma, then radiometric ages obtained for CLF rocks should bracket this range. The wide range of ^{40}Ar-^{39}Ar ages obtained for sills and plagioclase-clinopyroxene tholeiites in this study and reported in Loewen et al. (in review) indicate that it is unlikely that the CLF lavas were produced by a single melting event. The ages of 62.3 to 92.0 Ma for tholeiites, from 83.9 to 91.8 Ma for sills, and from 86.3 to 88.4 Ma for hyaloclastites cover a much larger timespan than the previously reported ages of 88-90 Ma for Curaçao rocks. Thus, if a single mantle plume is responsible for the petrogenesis of the CLF, a mechanism is needed that provides for melting of plume head material over the 30 m.y. age range obtained for the CLF.

Constraints on Source Composition and Melting

Variations in REE concentrations can be used to constrain the mantle source composition and melting conditions involved in magma generation. **Figure 5** shows bivariate plots of selected incompatible trace elements. These elements tend to be preferentially partitioned into the melt phase during partial melting, and thus concentrations of each would be expected to exhibit similar variations over time in magmas derived from a common mantle source. As demonstrated by **Figure 5**, the majority of CLF samples have approximately constant La/Yb and Nb/Zr ratios. This

suggests that the rocks of Curaçao are derived from a compositionally homogenous mantle source.

Chondrite-normalized rare earth element diagrams for CLF rocks with reliable ^{40}Ar-^{39}Ar plateau ages are shown in **Figure 6**. As demonstrated by **Figure 6**, REE patterns for Curaçao rocks are flat to slightly depleted in LREEs throughout the range of ages obtained for the CLF. The majority of CLF samples used in this research also plot within the Icelandic Array of Fitton et al. (1997), as shown in **Figure 7**. This suggests that, despite the large age range of the CLF samples, their trace element chemistry is not inconsistent with a plume-related source. However, a mantle plume model for the petrogenesis of the CLF would require a mechanism capable of producing the persistently flat LREE patterns observed in the rocks of the CLF over time.

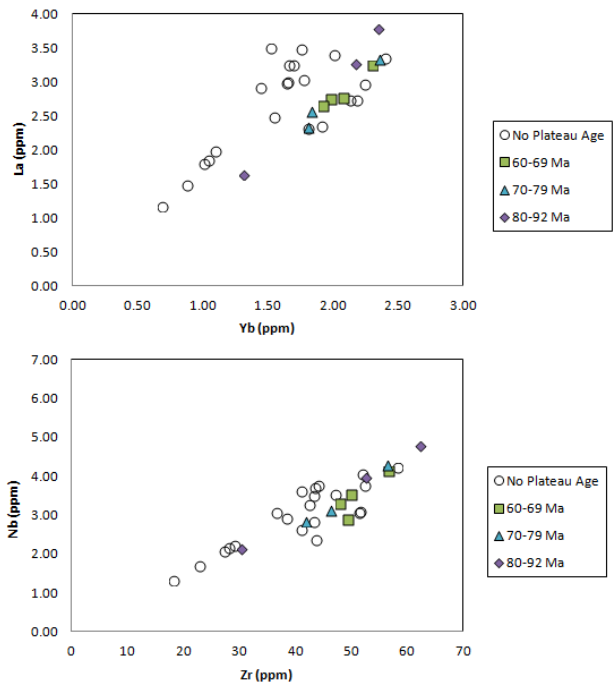

Figure 5. La-Yb (top) and Nb-Zr (bottom) plots of CLF samples.

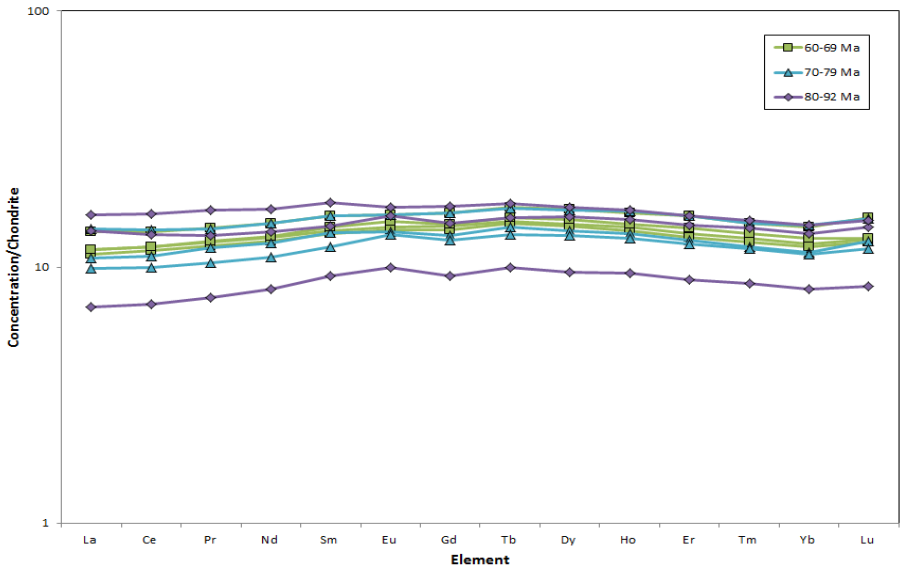

Figure 6. Rare earth element diagram of CLF samples of various ages. REE concentrations are normalized to C1 chondrite from McDonough and Sun (1995).

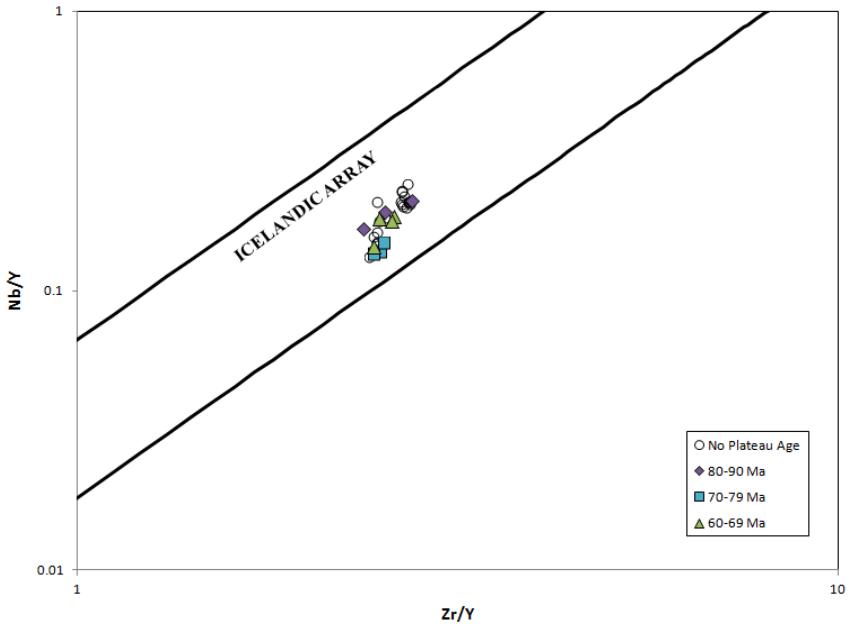

Figure 7. Nb/Y vs. Zr/Y plot of CLF samples of various ages. The majority of samples plot within the Icelandic Array of Fitton et al. (1997), suggesting a plume-related source.

Mantle Source Composition

In order to further test the validity of a plume-related model for the petrogenesis of the CLF, a batch melting model was used to determine if the range of REE compositions of the CLF rocks could be generated as a result of partial melting of a single mantle source. Primitive, enriched, and depleted mantle starting compositions from Gurenko and Chaussidon (1995) were used as the basis of the model. **Figure 8** shows batch melting models for Nb/Zr vs. La/Yb using the mantle source compositions in **Table 5** compared with a subset of Curaçao samples with reliable ^{40}Ar-^{39}Ar plateau ages. As demonstrated by **Figure 8**, the full range of compositions of CLF samples cannot be produced by partial melting of a pure enriched, depleted, or primitive source, or of a source consisting of a mixture of primitive and depleted components. The plot also demonstrates that, although the range of CLF compositions could be reproduced by melting of a source consisting of enriched and primitive components, it would require an unrealistically high degree of partial melting (~70-100%). Partial melting of a mantle source containing both enriched and depleted components, however, can produce the full range of CLF compositions plotted. **Figure 9** shows batch melting models of Nb/Zr vs. La/Yb using the compositions ED1 and ED2 in **Table 5** compared to the same CLF samples plotted in **Figure 8**. As demonstrated by **Figure 8,** the full range of REE concentrations observed in the rocks of the CLF can be reproduced by 10 to 30 percent partial melting of a predominately depleted source containing 1.4 to 3.4 percent of an enriched mantle component. This suggests that melting of a mantle source with an essentially homogenous composition (a hybrid mixture of predominantly depleted mantle

with a fraction of plume material) can account for the persistently flat LREE patterns observed in the rocks of the CLF.

Table 5. Mantle source compositions used in batch melting models, adapted from Gurenko and Chaussidon (1995). All concentrations are in µg/g.

Mantle Source	La	Ce	Nd	Sm	Eu	Dy	Yb	Nb	Zr
Depleted	0.310	0.950	0.860	0.320	0.130	0.635	0.425	0.280	8.400
Primitive	0.687	1.775	1.354	0.444	0.168	0.737	0.493	0.713	11.200
Enriched	5.000	11.810	7.710	2.470	0.710	2.810	1.460	13.100	61.400
ED1	0.469	1.319	1.093	0.393	0.150	0.709	0.460	0.716	10.202
ED2	0.376	1.102	0.956	0.350	0.138	0.665	0.439	0.459	9.142

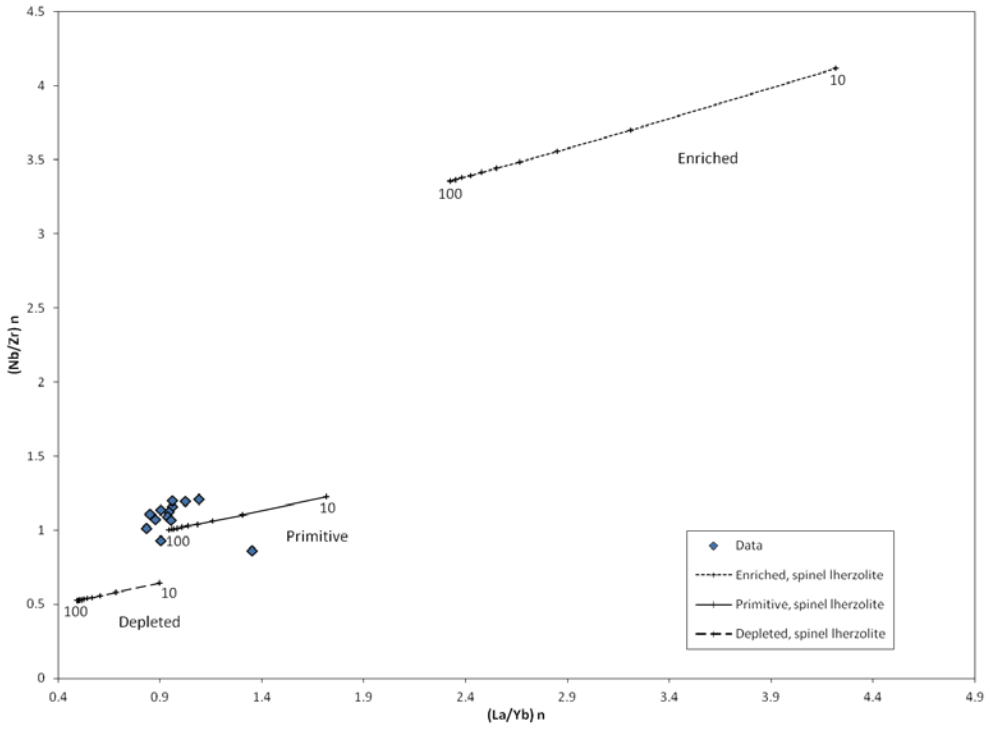

Figure 8. Batch melting models of Nb/Zr vs. La/Yb for enriched (top), primitive (middle) and depleted (bottom) mantle sources adapted from Gurenko and Chaussidon (1995). Source mineralogy is assumed to approximate spinel lherzolite. The models show concentrations from 10 to 100% melt, with each tick mark representing 10% melt (concentrations at melt fractions lower than 10% were omitted for ease of display).Trace element concentrations are normalized to C1 chondrite from McDonough and Sun (1995). Mantle source compositions are given in **Table 5**.

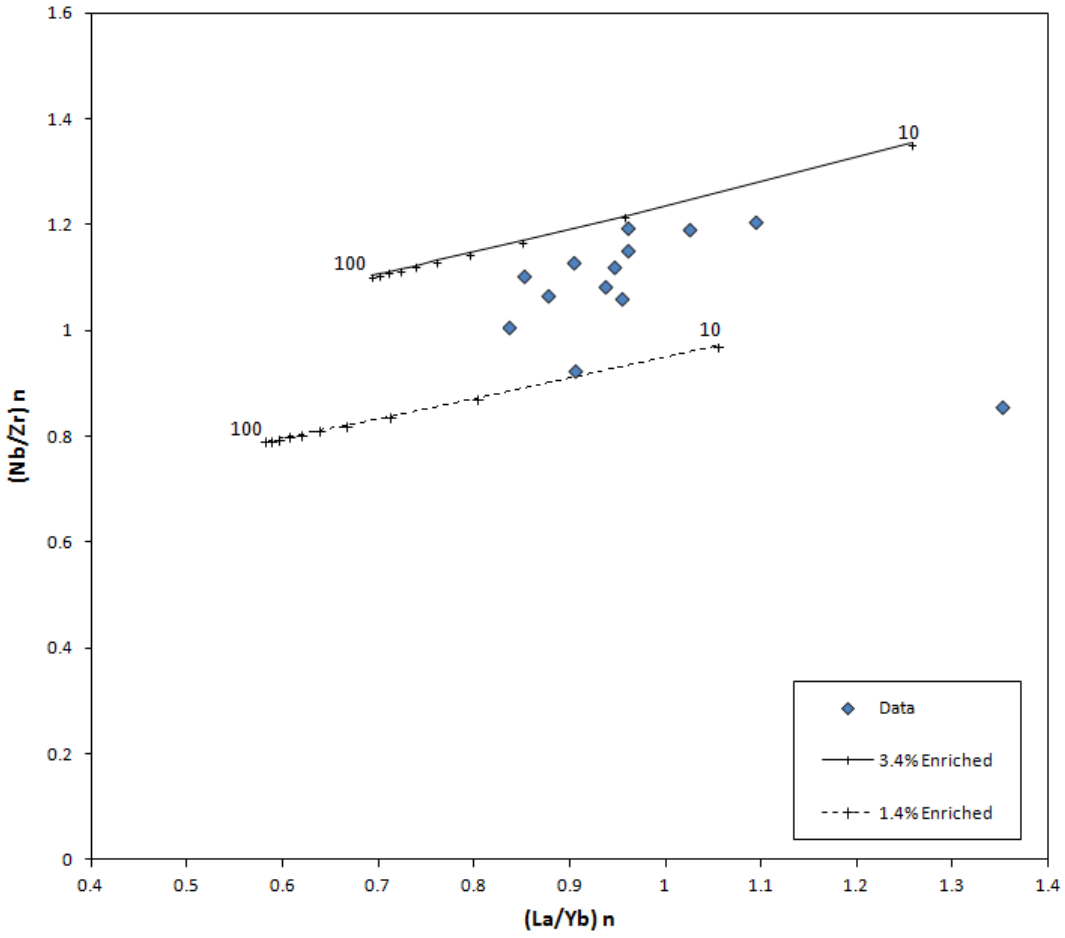

Figure 9. Batch melting models of Nb/Zr vs. La/Yb for mantle sources ED1 and ED2 from **Table 5** compared to CLF samples. Source mineralogy is assumed to approximate spinel lherzolite. The models show concentrations from 10 to 100% partial melt, with each tick mark representing 10% melt (concentrations at melt fractions lower than 10% were omitted for ease of display).Trace element concentrations are normalized to C1 chondrite from McDonough and Sun (1995).

Magma Evolution

Variation diagrams for selected major elements are shown in **Figure 10**. SiO_2, CaO, Al_2O_3, Na_2O, K_2O, and TiO_2 increase linearly from 29 to 9 wt% MgO, while Fe_2O_3* decreases linearly over the same range. These trends are consistent with olivine fractionation over this range of MgO contents, which extends from the picrites to the most primitive tholeiites. The trajectory of the increasing SiO_2 trend remains unchanged from 9 to 6 wt% MgO. Over this same range, Al_2O_3 and CaO decrease linearly, while Fe_2O_3*, Na_2O, and K_2O increase. TiO_2 increases linearly at a greater rate than over the previous range of MgO contents. These trends are consistent with plagioclase and clinopyroxene fractionation between 9 and 6 wt% MgO. The trends also indicate that olivine is no longer a major crystallizing phase over this range of MgO contents, which encompasses the full range of compositions of the sills and plagioclase-clinopyroxene tholeiites. Trends observed in the major element variation diagrams correlate well to previously observed trends for Curaçao rocks (Klaver, 1987).

Harker variation diagrams for Cr, Ni and Sr are shown in **Figure 11**. As in the major element variation diagrams, these trends compare well to previously observed trends for Curaçao rocks (Klaver, 1987). The steep linear decrease in Ni from 29 to 9 wt% MgO suggests that olivine and spinel are the dominant fractionating phases over this interval. However, the relatively high Ni content of several of the picrites suggests that this trend likely also reflects olivine accumulation. The conclusion that olivine and spinel are the first phases to crystallize is supported by petrographic observations, as the majority of olivine and spinel crystals observed in thin sections were euhedral. By 9 wt% MgO olivine is no longer a major fractionating phase, as indicated by the change in slope

of the Ni-MgO trendline from negative to approximately constant. At 9 wt% MgO, plagioclase and clinopyroxene become dominant fractionating phases, as evidenced by the decrease in slope observed in the Al_2O_3-MgO, CaO-MgO and Sr-MgO diagrams.

The most primitive picrite sample (CAO 15) was among the eight samples analyzed using EMPA. **Figure 12** shows a plot of whole rock FeO/MgO content vs. olivine FeO/MgO content for this sample. Olivine crystals formed in equilibrium with the surrounding melt would be expected to plot within the range of experimentally determined partition coefficients for FeO and MgO in basaltic systems ($K_d = 0.3 \pm 0.03$) as reported by Roeder and Enslie (1970). All of the olivine crystals tested have compositions that plot outside of this range, suggesting that much of the olivine in the sample did not crystallize in equilibrium with the surrounding liquid. This supports the conclusion of Kerr et al. (1996) that the high-MgO Curaçao picrites are olivine cumulates.

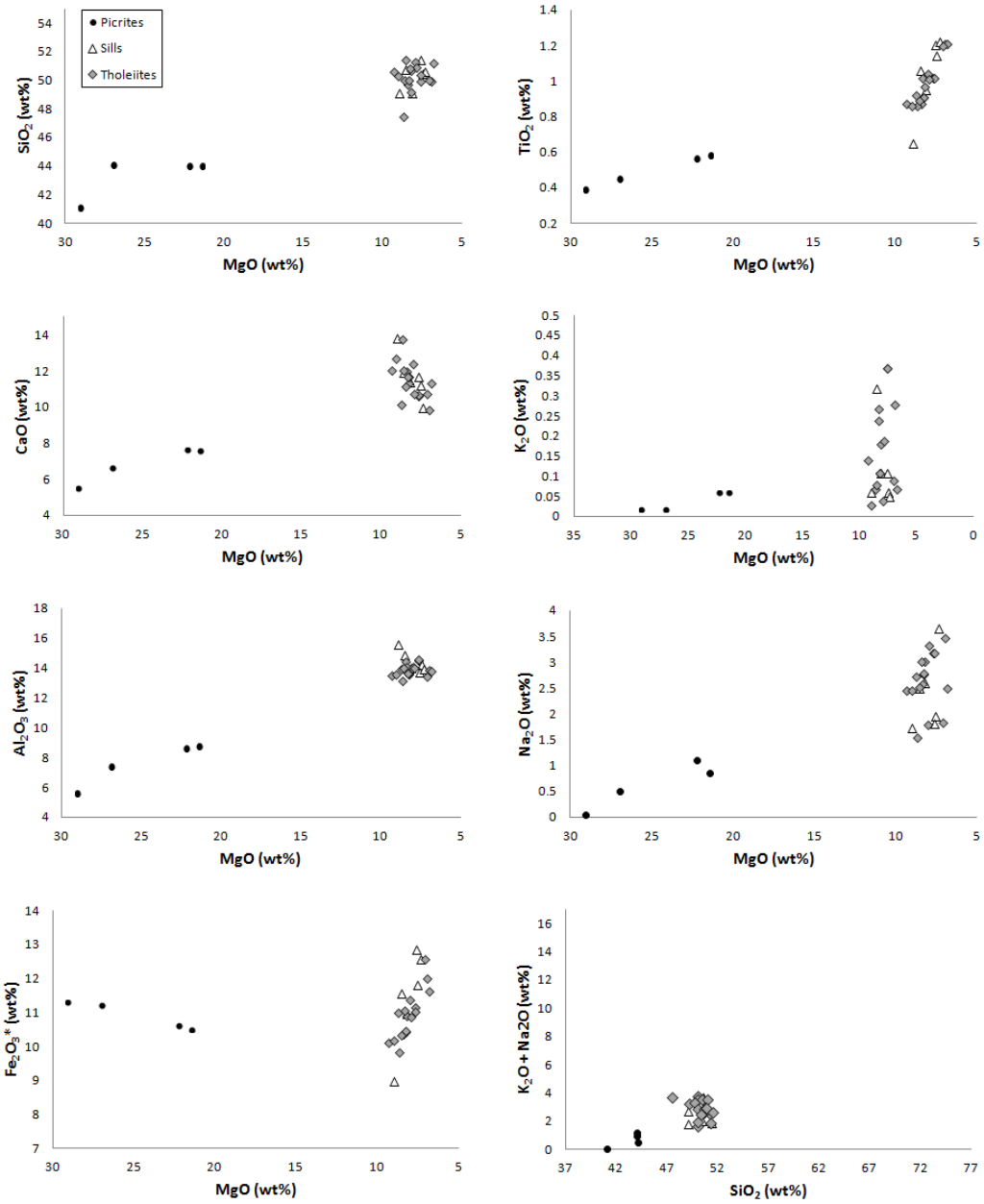

Figure 10. Major element variation diagrams for CLF samples.

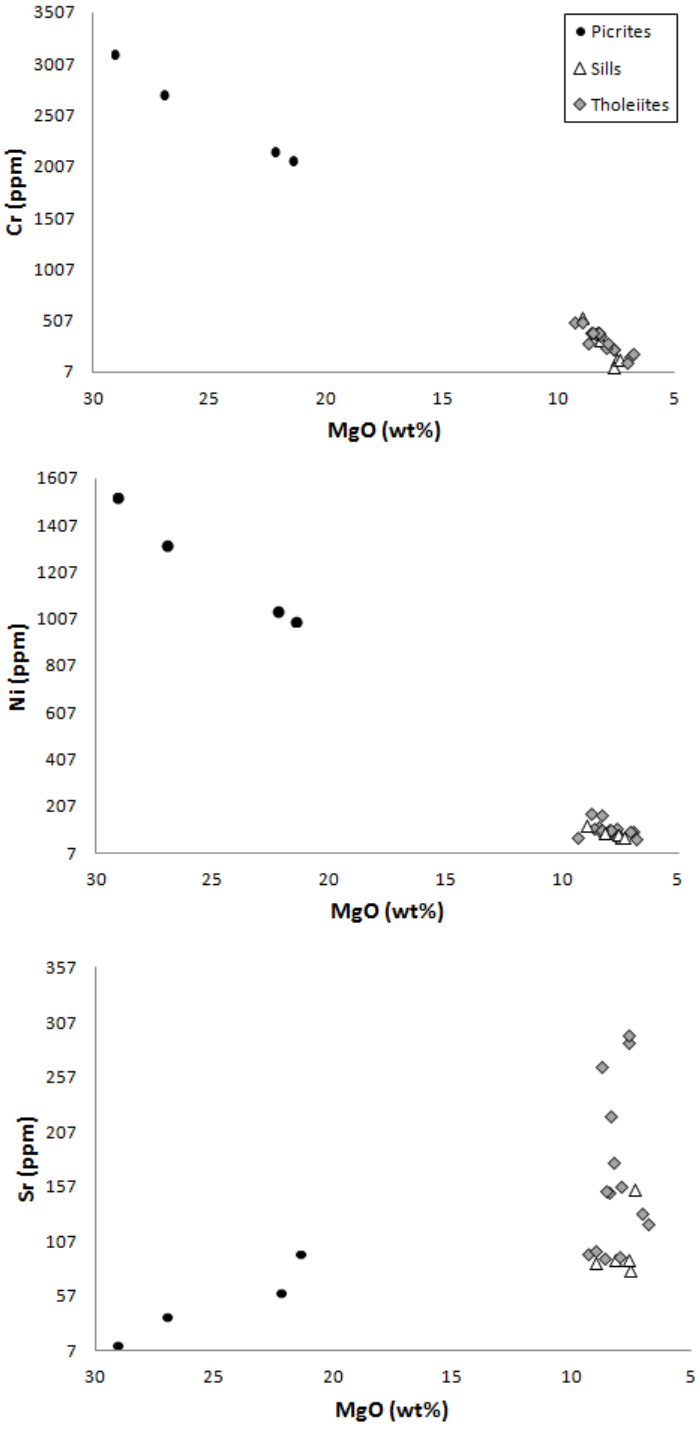

Figure 11. Trace element Harker diagrams for CLF samples.

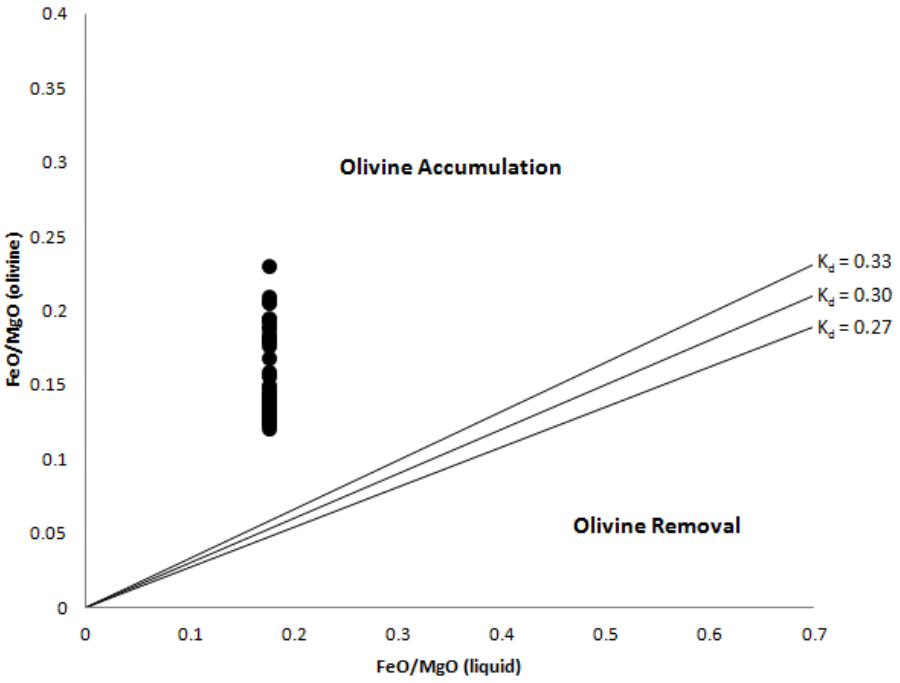

Figure 12. FeO/MgO content for olivine versus FeO/MgO content of liquid (calculated using FeO/MgO content of host rock) for sample CAO 15. Equilibrium lines for $K_d = 0.27$, $K_d = 0.30$, and $K_d = 0.33$ (Roeder and Enslie, 1970) are also shown. All olivine compositions plot outside of the field defined by the equilibrium lines, indicating that the crystals did not form in equilibrium with the surrounding liquid.

Crystallization trends generated by MELTS were compared to trends on major element variation diagrams. **Figure 13** shows the liquid line of descent calculated by the MELTS model compared to major element variation diagrams for Al_2O_3, FeO* and CaO plotted against MgO. These four oxides are the most abundant constituents in the dominant mineral phases (olivine, plagioclase, and clinopyroxene) identified in the Curaçao samples, and thus provide a good approximation of the model's validity. The starting composition used in this model falls within the range of compositions observed for CLF picrites. The crystallization trends predicted by this model correspond well to the

trends on these element variation diagrams. The slight deviation of the liquid line of descent predicted by the model for FeO* vs. MgO from the trends shown by XRF data may indicate that the starting composition used in the model has a higher Fe content than the actual parental magma. The general agreement between the crystallization trends shown by the MELTS model and XRF data suggests that the more evolved picrites, sills and plagioclase-clinopyroxene tholeiites could have been produced by fractional crystallization of a melt with 24 wt% MgO. The trends shown by the model indicate that olivine is crystallizing between 1520 ºC and 1180 ºC, and that clinopyroxene and plagioclase begin crystallizing at 1180-1220 ºC. These temperature ranges are similar to those reported by Klaver (1987) for Curaçao basalts (1440-1190 ºC for olivine, 1230 ºC to less than 1120 ºC for plagioclase, and 1215 ºC to less than 1120 ºC for clinopyroxene).

The same starting composition was used to model crystal fractionation under variable water contents, pressures, and oxygen fugacities (fO_2) in order to constrain the conditions under which the rocks of Curaçao formed. **Figure 14** shows variations in the liquid line of descent predicted by models with increasing parental magma H_2O content. Although additional water causes little change in crystallization trends on the CaO diagram, the trends predicted by the FeO* and Al_2O_3 diagrams change considerably. This is likely due to changes in the stability of pyroxene and plagioclase. The liquid line of descent produced by a model with an initial H_2O content of 0.1 wt% most closely matches the trends observed on the major element variation diagrams, suggesting that the parental magmas that formed the rocks on Curaçao were relatively dry. **Figure 15** shows variations in the liquid line of descent predicted by models under increasing pressure. The crystallization trends predicted by the CaO, Al_2O_3 and FeO* diagrams vary significantly

as pressure increases. The liquid lines of descent that most closely match the trends on the major element variation diagrams correspond to pressures of 1 to 2.5 kbar, which likely represents the maximum pressure under which the Curaçao parental magmas may have crystallized. **Figure 16** shows variations in the liquid line of descent predicted by models using different redox buffers to constrain oxygen fugacity (fO_2). Oxygen fugacity influences the redox state of iron in the magma, and will determine the stability of Fe^{2+} relative to Fe^{3+}. Crystallization trends on both the Al_2O_3 and FeO* diagrams show significant variation under different fO_2 conditions. The liquid line of descent produced by the model utilizing a quartz-magnetite-fayalite (QMF) redox buffer most closely matches the trends shown by the major element variation diagrams, and thus likely describes the fO_2 conditions under which the Curaçao parental magmas crystallized.

The MELTS models, along with the trace and major element variation diagrams, support the conclusion that the more evolved picrites, sills, and plagioclase-clinopyroxene tholeiites crystallized from parental magmas with 24 wt% MgO and broadly similar compositions. This observation is consistent with the conclusion that the melting conditions and composition of the mantle source of the Curaçao rocks remained relatively constant over the approximately 30 m.y. age range of the CLF.

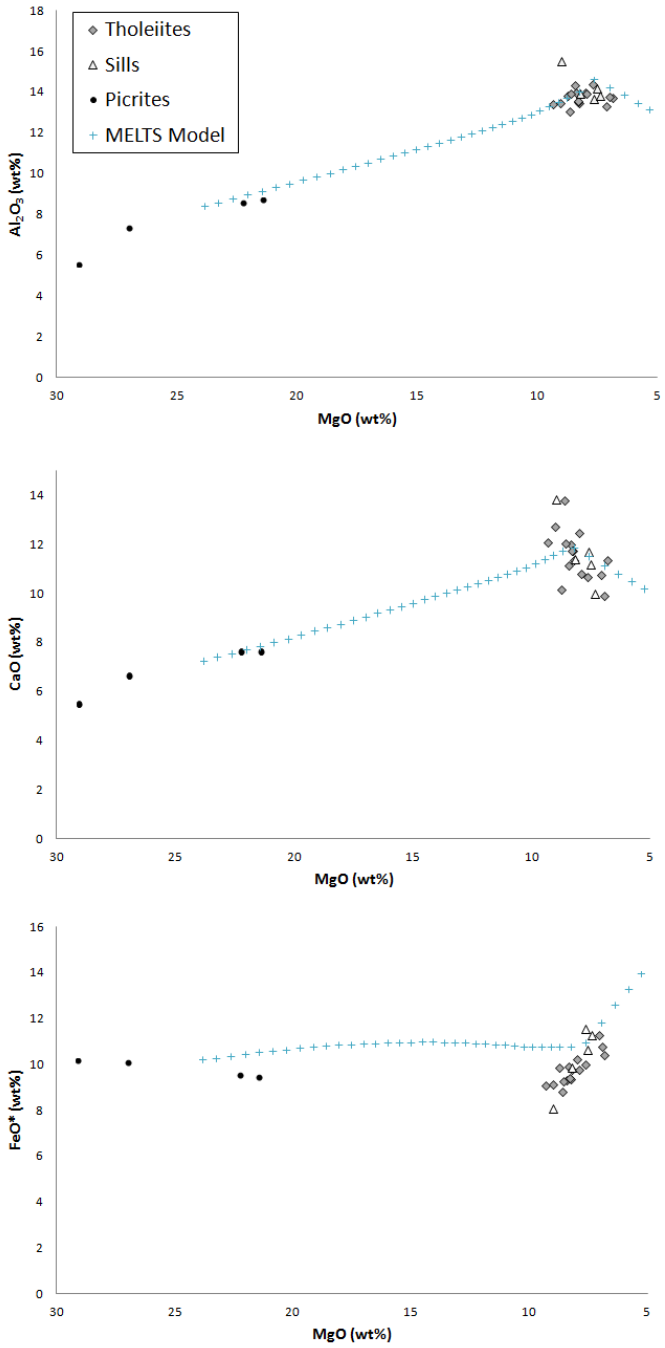

Figure 13. Liquid line of descent modeled by MELTS at 1 kbar, with oxygen fugacity constrained using the QMF redox buffer. The starting composition is given in **Table 1.**

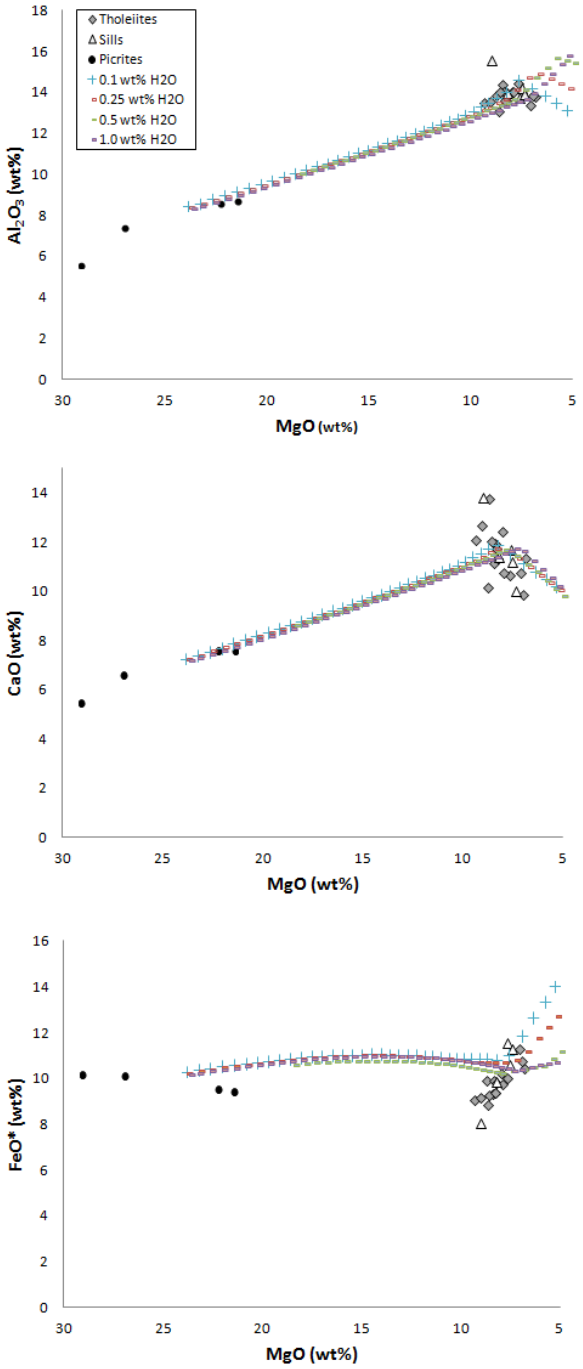

Figure 14. Liquid lines of descent modeled by MELTS at various water contents at 1 kbar, with oxygen fugacity constrained using the QMF redox buffer. The starting composition is given in **Table 1**. For water contents greater than 0.1 wt%, total oxide content was renormalized to 100%.

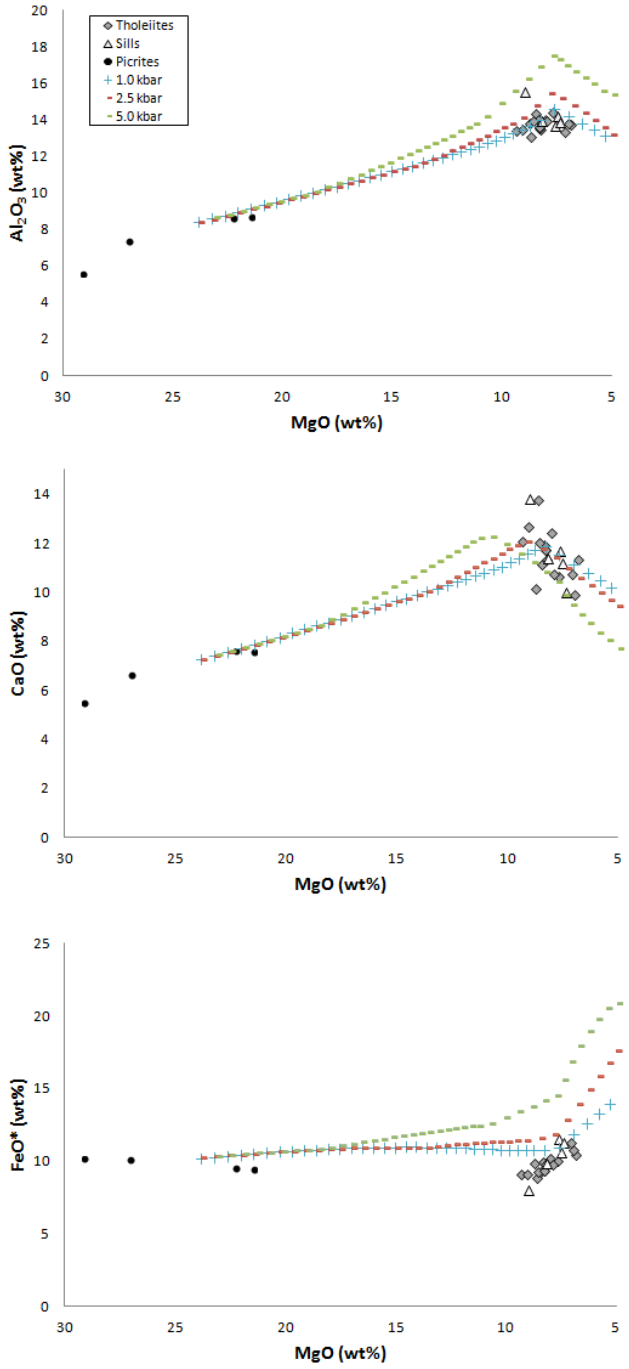

Figure 15. Liquid lines of descent modeled by MELTS at various pressures, with oxygen fugacity constrained using the QMF redox buffer. The starting composition is given in **Table 1**.

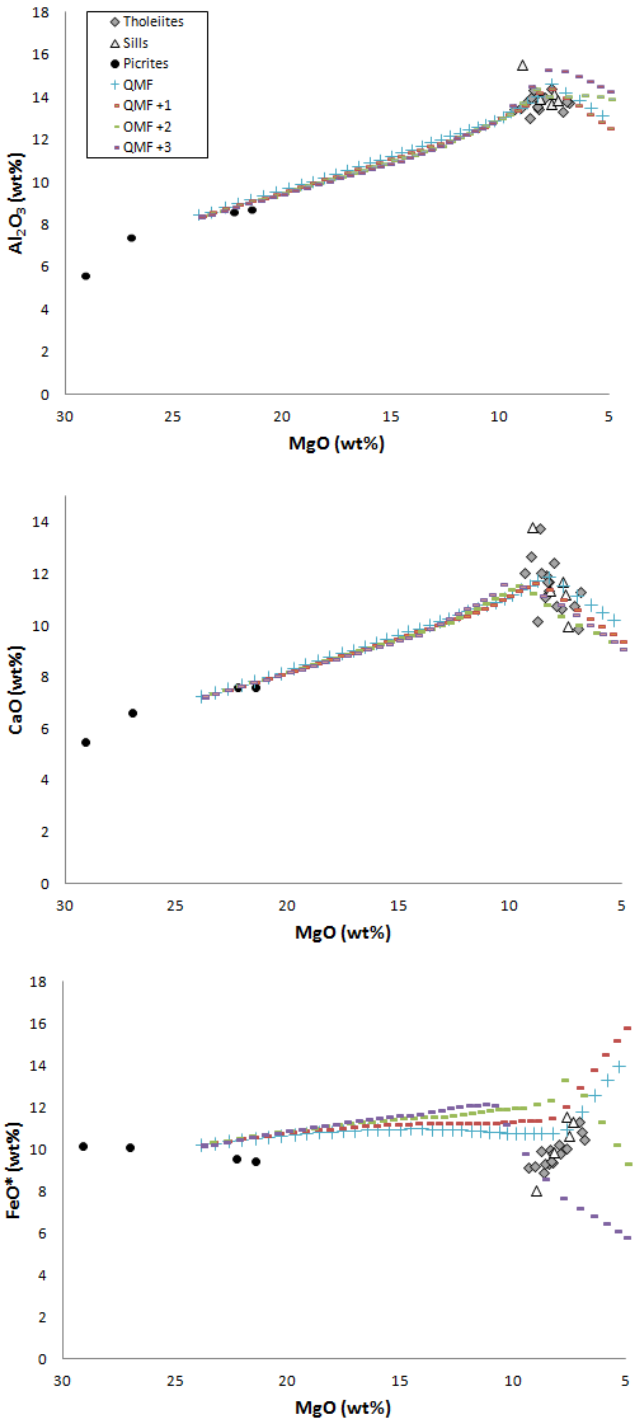

Figure 16. Liquid lines of descent modeled by MELTS using various redox buffers to constrain oxygen fugacity at a pressure of 1 kbar. The starting composition is given in **Table 1.**

Model for CLIP Formation

The data obtained over the course of this research challenge many of the previous models for the petrogenesis of the CLF. New ^{40}Ar-^{39}Ar ages ranging from 61 to 93 Ma indicate that the CLF did not form predominately at 88-90 Ma. However, the CLF samples utilized in this research plot within the Icelandic Array, consistent with formation from a plume-related source (Fitton et al., 1997). Additionally, batch melting models utilized as part of this research indicate that it is possible to produce the full range of REE compositions of the CLF rocks through 10 to 30 percent partial melting of a predominately depleted mantle lherzolite source containing a small amount (1.4 to 3.4 percent) of an enriched mantle component.

A consideration of the complicated tectonic history of the CLIP suggests a possible mechanism that could reproduce these results (**Figure 17**). A model developed by Loewen et al. (in review) utilizes the interactions between plumes and subduction zones through mantle flow to explain the origin of the CLIP. As noted by Richards and Griffiths (1989), mantle flow can result in the horizontal displacement of mantle plumes. Thus, following the polarity reversal of the Greater Antilles Arc at ~80-90 Ma, mantle flow associated with subduction at the now southwest-dipping trench would be expected to result in an eastward deflection of the head of the plume that formed the CLIP. As a result, the enriched plume head material would be advected through the depleted upper mantle beneath the CLIP, while the position of the plume tail would remain largely fixed beneath the western edge of the plateau. The subsequent formation of the northeast-dipping Central America Arc by 60 Ma would then result in the separation of the plume head from the tail, causing the former to be essentially isolated beneath the CLIP.

Northeast and southwest mantle flow generated by the Central America Arc and the Greater Antilles Arc would result in further lateral displacement of the plume head material beneath the CLIP. Thus, volcanism over the 30 million year age range of the CLF could repeatedly tap this plume head material. The volcanism that formed the CLIP may also have been mediated by extensional faulting. As noted by Ito and Clift (1989), multiple oceanic LIPs formed during the Cretaceous exhibit extensive normal faulting along margins and within their interiors.

As demonstrated by the models shown in **Figure 8** and **Figure 9**, the persistently flat LREE patterns observed in CLF rocks over the entire 30 million year age range can be generated by 10-30% partial melt of a predominately depleted mantle source with 1.4 to 3.4% of an enriched component. This mantle source is consistent with this model for the petrogenesis of the CLIP. The lateral displacement of enriched plume head material through the depleted upper mantle beneath the CLIP could potentially produce a predominately depleted source with a small contribution from an enriched component. The model for CLIP formation presented above is thus broadly consistent with the observed geochemical and geochronological trends of rocks from the CLF.

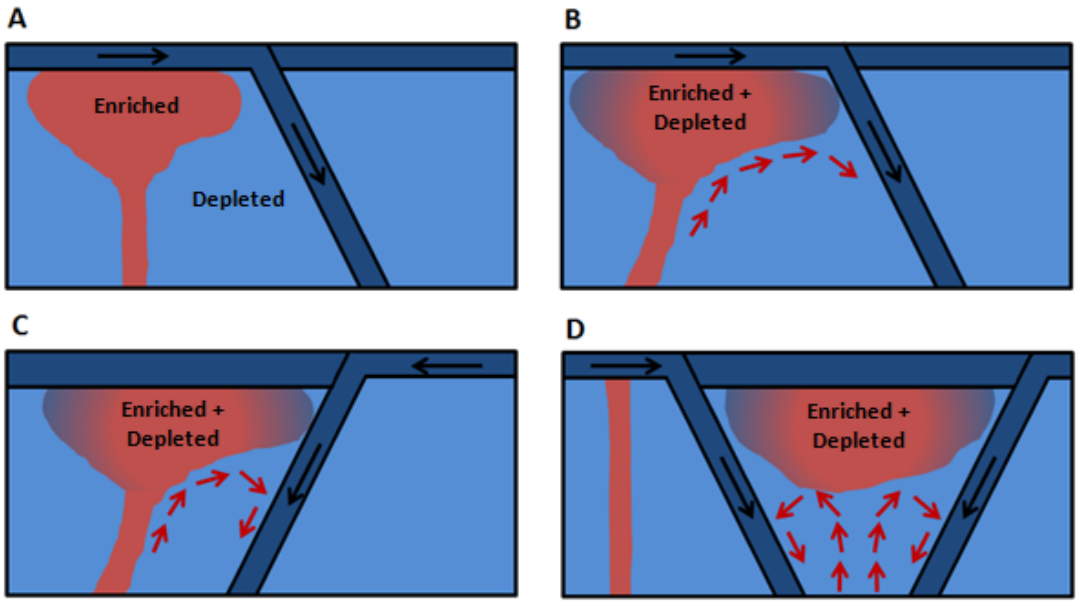

Figure 17. Conceptual model of CLIP petrogenesis. Part A shows mantle plume initiation at about 90 Ma. Part B shows the lateral displacement of the plume head driven by subduction-driven mantle flow, resulting in the incorporation of depleted upper mantle material into the enriched plume head. Part C shows the polarity reversal of the Greater Antilles Arc at 80-90 Ma and the resulting subduction beneath the Caribbean plateau. Part D shows the initiation of the Central American Arc at about 60 Ma, the separation of the plume head from the plume tail, and the resulting mantle flow regime beneath the Caribbean plateau.

IMPLICATIONS AND FUTURE WORK

The model presented in this research represents a departure from traditional conceptions of the petrogenesis of the CLF and CLIP. Previous models concluded that the petrogenesis of the Caribbean plateau occurred as a result of melting triggered by the arrival of a mantle plume over a geologically short time period at about 88-90 Ma. However, these models are incompatible with the approximately 30 million-year age range of CLF rocks. The flat REE patterns observed for CLF rocks over this age range appear to contradict the expected geochemistry of magmas derived from a progressively depleted mantle plume, but can be reproduced by 10 to 30 percent partial melting of a continually replaced, predominately depleted source with a minor enriched component. Modeling results also indicate that the primary magmas that formed the rocks of the CLF are of broadly similar composition.

The proposed petrogenetic model for the CLIP adequately describes the geochemical and geochronological trends observed for the CLF. Future research could examine the geochemistry and geochronology of other remnants of the Caribbean plateau (e.g. Haiti, the Beata Ridge, and Gorgona) in order to further refine the model and constrain the origin of the Caribbean plateau. Additionally, although this model provides constraints on the compositions of a mantle source and parental magmas for the CLIP, the composition of the primary magma(s) that formed the CLIP remain poorly constrained. Information about the composition and evolution of these primary magma(s) is essential to the development of a complete model of the petrogenesis of the Caribbean plateau.

BIBLIOGRAPHY

Beets, D.J., G.T. Klaver, F.F. Beunk, C. Kieft, and P. Maaskant, 1982. Picrites as parental magma of MORB type tholeiites. *Nature*, *296*, 341-343.

Burke, K.C., C. Cooper, J.F. Dewey, P. Mann, and J.L. Pindell, 1984. Caribbean tectonics and relative plate motions, in W.E. Bonini, R.B. Hargraves, and R. Shagam, eds., The Caribbean-South American plate boundary and regional tectonics. *Geological Society of America Mem., 162*, 31-63.

Coffin, M.F. and O. Edholm, 1994. Large igneous provinces: crustal structure, dimensions and external consequences. *Rev. Geophysics*, *32*, 1-36.

Duncan, R.A. and R.B. Hargraves, 1984. Plate tectonic evolution of the Caribbean region in the mantle reference frame, in W.E. Bonini, R.B. Hargraves, and R. Shagam, eds., The Caribbean-South American plate boundary and regional tectonics. *Geol. Soc. America Mem., 162*, 81-93.

Duncan, R.A. and M.A. Richards, 1991. Hotspots, mantle plumes, flood basalts, and true polar wander. *Rev. Geophysics*, *29*, 483-501.

Fitton, J.G., A.D. Saunders, M.J Norry, B.S. Hardarson, and R.N. Taylor, 1997. Thermal and chemical structure of the Iceland plume. *Earth and Planetary Science Letters*, *153*, 197–208.

Ghiorso, M. S., and R.O. Sack, 1995. Chemical mass transfer in magmatic processes IV. A revised and internally consistent thermodynamic model for the interpolation and extrapolation of liquid-solid equilibria in magmatic systems at elevated temperatures and pressures. *Contributions to Mineralogy and Petrology, 119(2-3)*, 197-212.

Gurenko, A. A., and M. Chaussidon, 1995. Enriched and depleted primitive melts included in olivine from Icelandic tholeiites: origin by continuous melting of a single mantle column. *Geochimica et Cosmochimica Acta, 59*, 2905-2917.

Graham, D.J. and N.G. Midgley, 2000. Graphical representation of particle shape using triangular diagrams: An Excel Spreadsheet Method. *Earth Surface Processes and Landforms*, *25*, 1473-1477.

Ito, G., and P. D. Clift, 1998. Subsidence and growth of Pacific Cretaceous plateaus. *Earth and Planetary Science Letters*, *161*, 85-100.

Kerr, A.C., J. Tarney, G.F. Marriner, G.T. Klaver, A.D. Saunders, and M.F. Thirlwall, 1996. The geochemistry and petrogenesis of the late-Cretaceous picrites and

basalts of the Curaçao, Netherlands, Antilles: A remnant of an oceanic plateau. *Contributions to Mineralogy and Petrology*, *124*, 29-43.

Kerr, A.C., M.A. Iturralde-Vinent, A.D. Saunders, T.L. Babbs, and J. Tarney, 1999. A new plate tectonic model of the Caribbean: Implications from a geochemical reconnaissance of Cuban Mesozoic volcanic rocks. *Bulletin of the Geological Society of America*, *111*, 1581-1599.

Klaver, G.T., 1987. The Curaçao lava formation: An ophiolitic analogue of the anomalous thick layer 2B of the mid-Cretaceous oceanic plateaus in the western Pacific and central Caribbean. Ph.D. dissertation, University of Amsterdam, The Netherlands, 168 p.

Koppers, A.A.P., 2002. ArArCALC - software for Ar-40/Ar-39 age calculations. *Computers & Geosciences*, *28(5)*, 605-619.

Larson, R.L. 1991. Geological consequences of superplumes. *Geology*, *19*, 963-966.

Loewen, M., R. A. Duncan, K. Krawl, and A.J.R. Kent, 2013. 30 Million Years of Plume Volcanism in the Caribbean Large Igneous Province. Manuscript in review.

McDonough, W. F. and S. S. Sun, 1995. The composition of the Earth. *Chemical Geology*, *120*, 223-253.

Morgan, W.J., 1981. Hotspot tracks and the opening of the Atlantic and Indian oceans, in *The Oceanic Lithosphere, The Sea*, ed. C. Emiliani, pp. 443-487, John Wiley and Sons, Hoboken, New Jersey.

Pindell, J.L. and S.F. Barrett, 1990. Geological Evolution of the Caribbean region: A plate tectonic perspective, in *The Geology of North Americ*a, *v. H, The Caribbean Region*, eds. G. Dengo and J.E. Case, pp. 405-432, Geological Society of America, Boulder, Colorado.

Renne, P.R., C.C. Swisher, A.L. Deino, D.B. Karner, T.L. Owens, and D.J. DePaolo, 1998. Intercalibration of standards, absolute ages and uncertainties in $^{40}Ar/^{39}Ar$ dating. *Chemical Geology*, *145*, 117–152.

Révillon, S., N.T. Arndt, E. Hallot, A.C. Kerr, and J. Tarney, 1999. Petrogenesis of picrites from the Caribbean Plateau and the North Atlantic magmatic province. *Lithos*, *49*, 1-21.

Richards, M.A., R.A. Duncan, and V.E. Courtillot, 1989. Flood basalts and hotspot tracks: Plume heads and tails, *Science*, *246*, 103-107.

Richards, M. A., and R.W. Griffiths, 1989. Thermal entrainment by deflected mantle plumes.: *Nature*, *342*, 900-902.

Roeder, P.L. and R.F. Enslie, 1970. Olivine-liquid equilibrium. *Contributions to Mineralogy and Petrology*, *29*, 275-289.

Sinton, C.W., R.A. Duncan, M. Storey, J. Lewis, and J.J. Estrada, 1998. An oceanic flood basalt province within the Caribbean plate. *Earth and Planetary Science Letters*, *155*, 221-235.

Steiger, R.H. and E. Jäger, 1977. Subcommission on geochronology: convention on the use of decay constants in geochronology and cosmochronology. *Earth and Planetary Science Letters, 36,* 359–362.

Walker, R.J., M.J. Storey, A.C. Kerr, J. Tarney, and N.T. Arndt, 1999. Implications of 187Os isotopic heterogeneities in a mantle plume: Evidence from Gorgona Island and Curaçao. *Geochemica et Cosmochemica Acta*, *63*, 713-728.